

**SPLIT MODE METHOD FOR THE ELLIPTIC  
2D SINE-GORDON EQUATION: APPLICATION TO  
JOSEPHSON JUNCTION IN OVERLAP GEOMETRY\***

JEAN-GUY CAPUTO

*Laboratoire de Mathématiques, Institut de Sciences Appliquées  
and U.R.A. C.N.R.S. 1378  
BP8, 76131 Mont-Saint-Aignan Cedex, France*

NIKOS FLYTZANIS

*Physics Department, University of Crete  
71409 Heraklion, Greece*

YURI GAIDIDEI

*Institute for Theoretical Physics  
252143 Kiev, Ukraine*

IRENE MOULITSA and EMMANUEL VAVALIS

*Mathematics Department, University of Crete  
71409 Heraklion, Greece  
and Institute of Applied and Computational Mathematics, FORTH  
71110 Heraklion, Greece*

Received 2 December 1997

Revised 21 Jan 1998

We introduce a new type of splitting method for semilinear partial differential equations. The method is analyzed in detail for the case of the two-dimensional static sine-Gordon equation describing a large area Josephson junction with overlap current feed and external magnetic field. The solution is separated into an explicit term that satisfies the one-dimensional sine-Gordon equation in the  $y$ -direction with boundary conditions determined by the bias current and a residual which is expanded using modes in the  $y$ -direction, the coefficients of which satisfy ordinary differential equations in  $x$  with boundary conditions given by the magnetic field. We show by direct comparison with a two-dimensional solution that this method converges and that it is an efficient way of solving the problem. The convergence of the  $y$  expansion for the residual is compared for Fourier cosine modes and the normal modes associated to the static one-dimensional

PACS Nos.: 74.50.+r, 02.60.Lj, 02.70.Dh.

\*Part of this work was supported by EEC grant SC1\*-CT91-0760 and a PENED grant (No. 2028/1995). Y. G. and J. G. C. acknowledge the hospitality of the University of Crete. The visit of J. G. C. was made possible by a grant under the Greek-French collaboration agreement. Y. G. received partial support from the grant K95100 of the International Science Foundation and the Government of Ukraine and from SRC QM "Vidhuk".

sine-Gordon equation and we find a faster convergence for the latter. Even for such large widths as  $w = 10$  two such modes are enough to give accurate results.

*Keywords:* Josephson Junctions, Partial Differential Equations; Solitons.

## 1. Introduction

Operator splitting methods have been introduced in the past few decades and proved to be an efficient way of solving high dimensional partial differential equations (PDE). Yanenko in his 1971 pioneering book<sup>1</sup> showed how to decompose linear operators along different directions to obtain the solution of a problem in two or three space dimensions. This idea of splitting linear operators has been widely used in applications and has been generalized to nonlinear time dependent problems where the operator is decomposed into a linear and a nonlinear part solved in alternating fashion.<sup>2</sup> While Yanenko's method involves only a splitting of the operator, a new method due to Adomian<sup>3</sup> specifically tailored to solve nonlinear problems uses a splitting both of the solution and the nonlinear operator in an expansion series. This method seems well adapted to solve initial value problems with polynomial nonlinearities<sup>4</sup> but it is not clear that it can be implemented for nonlinear boundary value problems. Here we present a method which can be applied to precisely this type of problem when it has some symmetries and an analytic solution in some limit. Following the ideas of Yanenko we decompose the linear space operator but also the solution and use the fact that for the parameter values giving a one-dimensional (1D) limit, the problem can be solved exactly. From physical considerations we write the solution as the sum of the solution of this auxiliary 1D problem plus a residual. Then as long as the parameters are not too far from the 1D case the problem can be treated perturbatively and therefore the amplitude of the residual remains small so that the intrinsic difficulties due to the nonlinearity have been reduced.

In Ref. 5 we have applied this split mode method (SMM) to solve the two-dimensional (2D) static sine-Gordon equation describing the superconducting phase for a wide area Josephson junction with overlap current feed. The boundary conditions are of Neumann type and involve both the external current and the applied magnetic field. An important quantity is the maximum current for which a stable solution exists for a given magnetic field. This measurement can serve as a characterization method of the junction. In Ref. 5 a cosine mode expansion was used for the  $y$  variation of the residual and we kept only two terms in the expansion for the numerical calculations. For the modal amplitudes we derived two equations the second of which was linearized. The method gave reasonable agreement with the 2D numerical solution for  $w < 6$  ( $w$  is the normalized width) and also asserted the validity of the commonly used one-dimensional model for  $w < 2$ . Here we show that this split mode method introduced from physical arguments is an efficient way of solving the problem and that control of the accuracy of the calculation is done by keeping as many terms in  $y$  as necessary. We also show that normal modes in

$y$  obtained by solving the linearized problem derived from the 1D sine-Gordon (the auxiliary problem) yield a faster convergence than cosine modes.

The paper is organized as follows. In Sec. 2 we briefly describe the PDE mathematical model and present the Split Mode method, where the coupling between  $x$  and  $y$  is treated in a mode expansion which transforms the 2D PDE problem into a system of ordinary differential equations (ODE) problem. In Sec. 3 we derive and study our normal mode expansion in  $y$  and compare it with a Fourier cosine expansion. In Sec. 4, numerical methods for solving the reduced model are described and their complexity analysis is presented and compared with the one associated with the numerical methods for solving the 2D PDE model. In Sec. 5 we present the numerical results and compare with the direct solution of the 2D problem, and in the final section we summarize our results.

## 2. 2D Model

We consider a large area Josephson junction which consists of two superconducting metal plates (parallel to the  $x - y$  plane) separated by a thin oxide layer. The electromagnetic behavior of such a system can be described by  $\Phi(x, y)$ , the phase difference of the order parameters in the two superconductors. If the thickness  $d_0$  of the oxide layer is small as compared with the London penetration depths in the two superconducting films  $\lambda_L$  a two-dimensional approach to this problem is quite satisfactory.<sup>6</sup> Then a consistent reduction of the Maxwell and Josephson equations leads to the two-dimensional static sine-Gordon equation

$$\nabla^2 \Phi = \sin \Phi, \quad (1)$$

where the  $\sin \Phi$  nonlinearity is due to the Josephson supercurrent tunneling<sup>7</sup> and the unit of length is the Josephson penetration length  $\lambda_J$ , which is much larger than  $\lambda_L$ . In this approach the effective magnetic field  $\mathbf{H}$  and local surface supercurrent are determined by the gradient of the phase difference  $\Phi$ , the first one having constant value contours normal and the second parallel to the phase gradient. Thus, the boundary conditions (BC) for Eq. (1) in the case of a rectangular junction of (normalized) length  $\ell$  and width  $w$ , with an external magnetic field  $H_e$  applied along the  $y$  axis and a current feed  $I$  along  $y$  (overlap geometry) are

$$\left. \frac{\partial \Phi}{\partial x} \right|_{x=\pm\ell/2} = H_e, \quad (2a)$$

$$\left. \frac{\partial \Phi}{\partial y} \right|_{y=\pm w/2} = \pm \frac{I}{2\ell}. \quad (2b)$$

The sine-Gordon equation (1) arises also in other contexts like the mechanics of surface waves on an elastic film fixed to a nonlinear substrate<sup>8</sup> or the description of the orientation angle for nematic liquid crystals.<sup>9</sup> In those situations the boundary conditions differ from (2) but it is fairly clear that the split mode method described below can be implemented in those cases as well.

In the general case Eq. (1) under the BC (2) can be solved by a 2D discretization and direct numerical solution by iteration. Such a procedure, however requires intensive computations, especially if one is interested in obtaining the maximum tunneling current. In this case one must solve Eq. (1) over a range of  $H_e, I$  values. Reducing the dimensionality by one is of tremendous help not only in decreasing the computation time but also to obtain a clearer picture for the composition of the magnetic flux structure. This can be achieved by splitting the solution of (1) into a term  $\Phi_0$  that satisfies the 1D equation derived from (1) with the boundary conditions (2) and a residual that satisfies homogeneous Neumann BC on the  $y = \pm w/2$  sides. When the magnetic field  $H$  is zero the solution is given by  $\Phi = \Phi_0$  and the residual is zero. For  $H \neq 0$  the residual is expanded over  $y$  modes, the coefficients of which satisfy a system of coupled ODEs. We have shown in Ref. 5 that for a very narrow junction the solution is given as expected by the current driven sine-Gordon equation

$$\Phi_{xx} = \sin \Phi - \frac{I}{\ell w}. \quad (2)$$

The auxiliary problem derived from (1) is

$$\frac{d^2 \Phi_0(y)}{dy^2} = \sin \Phi_0(y), \quad (3)$$

with the boundary condition

$$\left. \frac{d\Phi_0}{dy} \right|_{y=\pm w/2} = \pm \frac{I}{2\ell}, \quad (4)$$

which can be seen as the problem of a 1D Josephson junction with inline current feed for zero external magnetic field. The solution of this problem is well known<sup>1,10</sup> and can be expressed explicitly in terms of Jacobi elliptic functions as

$$\sin \Phi_0 = 2\sqrt{m m_1} \operatorname{cd}(y|m) \operatorname{nd}(y|m), \quad (5)$$

$$\cos \Phi_0 = 2m \operatorname{cd}^2(y|m) - 1, \quad (6)$$

$$\frac{d\Phi_0}{dy} = 2\sqrt{m m_1} \operatorname{sd}(y|m), \quad (7)$$

where  $pq(y|m)$  with  $(p, q = s, c, d, n)$  are Jacobi elliptic functions with modulus  $m$  ( $m_1 = 1 - m$  is the complementary modulus).<sup>11</sup> The period of the elliptic functions is  $4K(m)$  (except for  $dn$  which is  $2K(m)$ ) where

$$K(m) = \int_0^{\pi/2} d\phi (1 - m \sin^2 \phi)^{-1/2} \quad (8)$$

is the complete elliptic integral of the first kind. The modulus  $m$  can be obtained from the boundary condition (4)

$$2\sqrt{m m_1} \operatorname{sd} \left( \frac{w}{2} \middle| m \right) = \frac{I}{2\ell}. \quad (9)$$

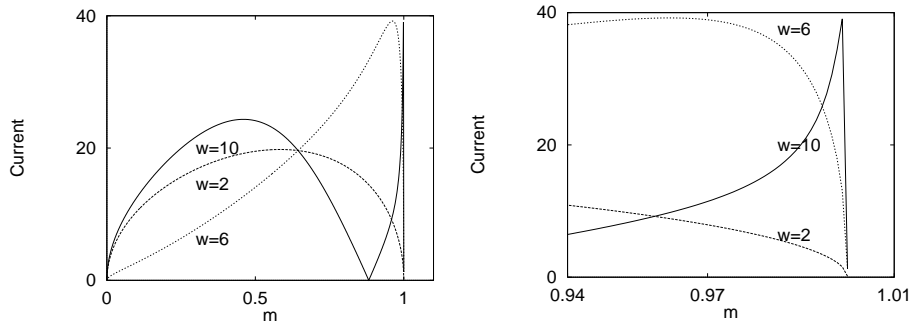


Fig. 1. Plot of  $I(m)$  from the l.h.s. of Eq. (10) for three values of  $w = 2, 6, 10$  on the left; on the right we expanded the scale near  $m = 1$ .

In Fig. 1 we plot  $I(m)$  from (9) for  $w = 2, 6, 10$ . We see that for  $w < 2\pi$  there is only one lobe while for  $w = 10$  there are two lobes. The second lobe is obtained by shifting the origin of  $y$  by  $2K(m)$  in Eqs. (5)–(7) and (9). This has the effect that there is an extra minus sign in the r.h.s of (9), so that the current is positive. In general every time  $w$  increases by  $2\pi$  we get an extra lobe. Since we are interested in the maximum current the part that will be of interest to us is the peak of the right lobe which will be approached from the right, where the solutions are stable to perturbations. To see the full lobe for  $w = 10$  we expand the scale near  $m = 1$ , so that the part of the  $w = 10$ , curve which appears as an almost vertical line in the normal scale, is seen to have a small but finite width.

Because the last lobe for large  $w$  is very steep it is useful to give some analytic formulas valid near  $m = 1$  and for the maximum point. By using asymptotic expressions and assuming that  $m_1 = 1 - m \approx \epsilon^2$ , where  $\epsilon$  is a small parameter we obtain from (9) the value of  $m_1$  where  $I$  is a maximum as

$$m_1^{\max} = \frac{4}{\sinh^2 \frac{w}{2}}. \quad (10)$$

The result is consistent with our scaling assumption

$$\frac{1}{\sinh \frac{w}{2}} \sim \epsilon. \quad (11)$$

In the above derivation care is required when simplifying the analytic formulas (Abramowitz, p. 574<sup>11</sup>) since near  $m = 1$  the elliptic functions are hyperbolic-like and when evaluated near  $y = w/2$  they affect the order of each term. The corresponding maximum current is

$$I = 4 - \frac{8}{\sinh^2 \frac{w}{2}}. \quad (12)$$

So that for a large junction width  $w$  it approaches exponentially the infinite length limit. In the absence of an external magnetic field,  $\Phi_0(y)$  is the full solution and its stability can be checked by looking for small perturbations around  $\Phi_0(y)$ .

The function  $\Phi_0(y)$  includes the dominant  $y$  dependence of the phase  $\Phi(x, y)$  and satisfies the external current boundary conditions for the overlap geometry. The full solution can be sought for in the form

$$\Phi(x, y) = \Phi_0(y) + \Psi(x, y), \quad (13)$$

where  $\Psi(x, y)$  satisfies

$$\nabla^2 \Psi = \sin[\Phi_0(y) + \Psi(x, y)] - \sin[\Phi_0(y)], \quad (14)$$

$$\left. \frac{\partial \Psi}{\partial x} \right|_{x=\pm \ell/2} = H_e, \quad (16a)$$

$$\left. \frac{\partial \Psi}{\partial y} \right|_{y=\pm w/2} = 0, \quad (16b)$$

where  $\Psi(x, y)$  now satisfies homogeneous BC at  $y = \pm w/2$ .

The solution of Eq. (1) under the boundary conditions (2) must be a symmetric function of the transversal variable  $y$  so that the function  $\Psi(x, y)$  is also symmetric. We can therefore represent  $\Psi(x, y)$  by a Fourier series in  $y$  which satisfies the boundary condition (16b).<sup>5</sup> Alternatively we can choose another complete set that satisfies the same boundary conditions in the  $y$  direction. For this purpose it is useful to select the complete set of the linearized normal modes around the  $y$ -dependent function  $\Phi_0(y)$ . It will be shown in the following that the two approaches are identical in the limit of small currents, while the linearized modes give a faster converging expansion near  $H = 0$ . In the following we present both expansions.

### 3. Split Normal Mode Expansion

The natural choice for a complete set of functions  $X_x(y)$  are the eigenmodes obtained from the linearized sine-Gordon equation (14) around the static solution  $\Phi_0(y)$ . By separation of variables we obtain the eigenvalue for the  $y$ -dependent part in the form

$$-X_n''(y) + \cos[\Phi_0(y)]X_n(y) = \lambda_n X_n(y), \quad (17)$$

with the boundary conditions

$$X_n'(y)|_{y=\pm w/2} = 0, \quad (18)$$

where “ $'$ ” denotes differentiation with  $y$ . The solution of the above eigenvalue problem will give a complete set of eigenfunctions  $X_n(y)$  with eigenvalues  $\lambda_n$ . We stress here that from the whole set of eigenmodes of the linearized problem the  $X_n$  are only the symmetric ones (in accordance with the symmetry of the potential  $\cos \Phi_0(y)$  in (17) and the BC in (18)) and are labeled consecutively  $n = 1, 2, \dots$ .

We did not consider the antisymmetric eigenmodes because they do not contribute to the following expansion (see Eq. (19)).

In the complete set  $X_n(y)$  we can expand the solution of (14)

$$\Psi(x, y) = \sum_{n=1}^{\infty} B_n(x) X_n(y), \quad (19)$$

where the coefficients  $B_n(x)$  are determined by the relations

$$B_n(x) = \int_{-w/2}^{w/2} dy \Psi(x, y) X_n(y), \quad (20)$$

i.e., we assumed that the modes  $X_n(y)$  are orthogonal and normalized to unity

$$\int_{-w/2}^{w/2} dy X_n(y) X_{n'}(y) = \delta_{nn'}. \quad (21)$$

Substituting Eq. (19) into Eq. (14) and using the notation  $B' \equiv \frac{dB}{dx}$  we get

$$\sum_{n=1}^{\infty} [B_n''(x) X_n(y) + B_n(x) X_n''(y)] = \sin \left[ \Phi_0(y) + \sum_{n=1}^{\infty} B_n(x) X_n(y) \right] - \sin \Phi_0. \quad (22)$$

Projecting Eq. (22) on the  $X_n(y)$  eigenmode and using the eigenvalue equation (17) and the normalization condition (21) we have for  $n = 1, 2, \dots$

$$B_n''(x) = \lambda_n B_n(x) - \sum_{n'=1}^{\infty} C_{nn'} B_{n'}(x) + \int_{-w/2}^{w/2} dy X_n(y) \left( \sin \left[ \Phi_0(y) + \sum_{n'=1}^{\infty} B_{n'}(x) X_{n'}(y) \right] - \sin \Phi_0 \right), \quad (23)$$

where

$$C_{nn'} = \int_{-w/2}^{w/2} dy \cos[\Phi_0(y)] X_n(y) X_{n'}(y). \quad (24)$$

The 2D problem now is reduced to the solution of the set of ODEs for the modal amplitudes  $B_n(x)$  with BC that depend on the external magnetic field, i.e.,

$$B_n' \left( \pm \frac{\ell}{2} \right) = H_n, \quad (25)$$

where  $H_n$  is the projection of the external magnetic field on the  $n$ -th eigenmode,

$$H_n = \int_{-w/2}^{w/2} dy H_e X_n(y). \quad (26)$$

In Sec. 5 we will present the numerical solution of the ODE system for arbitrary widths  $w$  and external magnetic fields. One can obtain simplified expressions for

small external magnetic field  $H_e$  where the amplitudes  $B_n(x)$  are small and we can expand the trigonometric functions in Eq. (23) into a series up to the fourth power, so that

$$B_n''(x) = \lambda_n B_n(x) - \frac{1}{2} \sum_{n'n''}^{\infty} s_{nn'n''} B_{n'}(x) B_{n''}(x) - \frac{1}{3!} \sum_{n'n''n'''}^{\infty} c_{nn'n''n'''} B_{n'}(x) B_{n''}(x) B_{n'''}(x), \quad (27)$$

$$s_{nn'n''} = \int_{-w/2}^{w/2} dy \sin[\Phi_0(y)] X_n(y) X_{n'}(y) X_{n''}(y), \quad (28)$$

$$c_{nn'n''n'''} = \int_{-w/2}^{w/2} dy \cos[\Phi_0(y)] X_n(y) X_{n'}(y) X_{n''}(y) X_{n'''}(y). \quad (29)$$

Near  $H_e = 0$  the dominant part of the solution is given by  $\Phi_0(y)$  and all  $B_n(x)$  are small. In this case one expects that high order in  $B_n(x)$  nonlinear terms are not important and for medium width  $w$  junctions only two terms in the expansion will contribute with eigenvalues  $\lambda_1, \lambda_2$  (with  $\lambda_1 < \lambda_2$ ) and amplitudes  $B_1(x)$  and  $B_2(x)$  correspondingly.  $B_1$  corresponds to the lowest eigenvalue and  $B_2$  to the next one associated with a symmetric eigenfunction. It is important to stress that at  $H_e = 0$ , when  $I$  becomes equal to  $I_{\max}$  ( $H_e = 0$ ), then  $\lambda_1$  becomes equal to zero. Therefore using only two modes we obtain

$$B_1''(x) = \lambda_1 B_1(x) - \frac{1}{2} s_{111} B_1^2(x) - s_{112} B_1(x) B_2(x) - \frac{1}{2} s_{122} B_2^2(x) - \frac{1}{6} c_{1111} B_1^3(x) - \frac{1}{2} c_{1112} B_1^2(x) B_2(x) - \frac{1}{2} c_{1122} B_1(x) B_2^2(x) - \frac{1}{6} c_{1222} B_2^3(x), \quad (30)$$

$$B_2''(x) = \lambda_2 B_2(x) - \frac{1}{2} s_{112} B_1^2(x) - s_{212} B_1(x) B_2(x) - \frac{1}{2} s_{222} B_2^2(x) - \frac{1}{6} c_{1112} B_1^3(x) - \frac{1}{2} c_{1122} B_1^2(x) B_2(x) - \frac{1}{2} c_{1222} B_1(x) B_2^2(x) - \frac{1}{6} c_{2222} B_2^3(x). \quad (31)$$

It is interesting to remark here that Eqs. (27) and (26) are the Euler–Lagrange equations for the functional

$$E = \sum_n \int_{-\ell/2}^{\ell/2} dx \left\{ \frac{1}{2} (B_n')^2(x) + \frac{1}{2} \lambda_n B_n^2 + H_n B_n(x) \left( \delta \left( x + \frac{\ell}{2} \right) - \delta \left( x - \frac{\ell}{2} \right) \right) \right\} - \frac{1}{3!} \sum_{n_1 n_2 n_3} \int_{-\ell/2}^{\ell/2} dx s_{n_1 n_2 n_3} B_{n_1} B_{n_2} B_{n_3} - \frac{1}{4!} \sum_{n_1 n_2 n_3 n_4} \int_{-\ell/2}^{\ell/2} dx c_{n_1 n_2 n_3 n_4} B_{n_1} B_{n_2} B_{n_3} B_{n_4}. \quad (32)$$

In the two mode approximation (30)–(31) it reduces to

$$\begin{aligned}
E = & \int_{-\ell/2}^{\ell/2} dx \left\{ \frac{1}{2} [(B_1')^2 + (B_2')^2] + \frac{1}{2} [\lambda_1 B_1^2 + \lambda_2 B_2^2] \right. \\
& + \sum_{n=1,2} H_n B_n(x) \left( \delta \left( x + \frac{\ell}{2} \right) - \delta \left( x - \frac{\ell}{2} \right) \right) \\
& - \frac{1}{3!} s_{111} B_1^3 - \frac{1}{2} s_{112} B_1^2 B_2 - \frac{1}{2} s_{122} B_1 B_2^2 - \frac{1}{6} s_{222} B_2^3 \\
& - \frac{1}{24} c_{1111} B_1^4 - \frac{1}{6} c_{1112} B_1^3 B_2 - \frac{1}{4} c_{1122} B_1^2 B_2^2 \\
& \left. - \frac{1}{6} c_{1222} B_1 B_2^3 - \frac{1}{24} c_{2222} B_2^4 \right\}. \tag{33}
\end{aligned}$$

The polynomial expansion is limited for  $B_n(x) < \pi$  and is valid only near  $H = 0$ , and elsewhere a numerical solution of (23) is required. We hope, however that only a small number of modes might be sufficient, while the symmetry of the problem eliminates the odd eigenfunctions of (17).

### 3.1. Comparison with Fourier cosine expansion

One can also consider various basis functions to expand  $\Psi(x, y)$  which over some range of parameters can have computational advantages. The fact that the  $X_n$  are eigenvectors of the linearized auxiliary problem in (17) simplifies the linear part in the equations for  $B_n(x)$  for small magnetic fields as can be seen from Eq. (23), where the coefficient of the linear term is  $\lambda_n$ , i.e., the eigenvalue of the corresponding eigenmode. There is also no linear coupling between different modes, but only in the nonlinear terms. The disadvantage is that even the first term in the expansion that contains the mode  $X_1(y)$  is  $y$ -dependent. This means that one can obtain simple 1D equations with simple coefficients only when  $B_1(x)$  is small and one can expand in Taylor series the trigonometric functions. Then instead of the integrated forms in (23) where the integrals have to be performed for each iteration, we obtain the simpler forms where the integrals are done once for each current and magnetic field in the coefficients  $s_{nn'n''}$  and  $c_{nn'n''n''}$ . This simplification is only in the formulation and does not increase the computational complexity. We will present in the following an efficient procedure to integrate the full equations (23) before the polynomial expansion.

An alternative to the eigenmodes in (17) is the complete set of cosine modes associated with the spectral problem,  $X_n''(y) = (\lambda_n - 1)X_n$  and the same BC as before. It is obtained by setting  $\cos \Phi_0 = 1$  in (17). This was proposed and formulated with only two modes in Ref. 5 with  $\Psi(x, y)$  given in the form

$$\Psi(x, y) = \sum_{n=1}^{\infty} A_n(x) \cos \frac{2\pi(n-1)y}{w}, \tag{34}$$

where the coefficients  $A_n(x)$  are obtained by projecting on the orthogonal basis functions (we take only the symmetric ones). When  $I \approx 0$ ,  $\Phi_0$  is close to zero so that the two sets of modes should be identical. The expansion (34) has the advantage over the previous  $X_n$  that the  $n = 1$  term is  $y$ -independent, so that under conditions where only that term is important, the coefficient  $A_1(x)$  satisfies a simple perturbed 1D sine-Gordon equation. Substituting Eq. (34) into Eqs. (14) and (16b) and using the notation  $\partial_x \equiv \partial/\partial x$  we get

$$\begin{aligned} \partial_x^2 A_n(x) - \left( \frac{2\pi(n-1)}{w} \right)^2 A_n(x) &= \frac{2 - \delta_{n,1}}{w} \int_{-w/2}^{w/2} dy \cos \frac{2\pi(n-1)y}{w} \\ &\times \left\{ \sin \left[ \Phi_0(y) + \sum_{n=1}^{\infty} A_n(x) \cos \frac{2\pi(n-1)y}{w} \right] - \sin \Phi_0(y) \right\}, \end{aligned} \quad (35)$$

$$\partial_x A_n \left( \pm \frac{\ell}{2} \right) = \delta_{n,1} H_e \quad n = 1, 2, \dots, \quad (36)$$

where  $\delta_{nn'}$  is the Kronecker delta.

By keeping only the term with  $A_1$  we get

$$\partial_x^2 A_1 = C_1 \sin A_1 + S_1 \cos A_1 - S_1, \quad (37)$$

where  $S_1$  and  $C_1$  are special cases for  $n = 1$  of the quantities

$$S_n = \frac{1}{w} \int_{-w/2}^{w/2} dy \sin[\Phi_0(y)] \cos \frac{2\pi(n-1)y}{w} \quad (38)$$

and

$$C_n = \frac{1}{w} \int_{-w/2}^{w/2} dy \cos[\Phi_0(y)] \cos \frac{2\pi(n-1)y}{w}. \quad (39)$$

Equation (37) reduces to the effective 1D model  $\partial_x^2 A_1 = \sin A_1 - S_1$ , if we put  $C_1 = 1$  and neglect the term  $S_1 \cos A_1$ . This is the case when the bias current is close to zero, so that  $\Phi_0$  is small and proportional to the external current density. Then one is allowed to average over  $y$  and obtain  $\langle \sin \Phi_0 \rangle \approx I/\ell w$ ,  $\langle \cos \Phi_0 \rangle \approx 1 + \mathcal{O}(I^2)$ , where  $\langle Q \rangle \equiv 1/w \int_{-w/2}^{w/2} dy Q(y)$ . In particular for all  $w$ 's at  $I = 0$  we have that  $\Phi_0 = 0$  so that  $\Phi = A_1$  and (37) reduces to the 1D static sine-Gordon equation (2), with zero bias current. At finite  $I$  we can consider only the case when  $w$  is small, where near  $I = I_{\max}$  (which for  $H = 0$  is  $I = \ell w$ ) we have  $\Phi \approx \pi/2$  and  $A_1 = 0$ . When this is introduced in (37) we get an identity while the same is true from (2). The crucial assumption here was that  $\Phi = \pi/2$  everywhere, which is of course not true for large  $w$ . In (38) and (39) we see that if only the term  $n = 1$  is kept in the summation, the integrations over  $y$  can be done analytically. This simplicity is lost however if the rest of the coefficients  $A_n$  are large, and one is again forced to do the integrals over  $y$  numerically for each iteration with a change in the bias current.

When an external magnetic field is absent ( $H_e = 0$ ) the problem is 1D (all  $A_n(x) = 0$ ) with  $\Phi(y)$  the complete solution with  $\Phi_0(y)$  the complete solution and the current and magnetic field distributions are described by Eqs. (10) and (11). The maximum current that goes through the barrier can be obtained from Eq. (9). For finite  $H_e$  the maximum current which flows through the barrier is decreased in a way which is implicitly determined by the boundary condition (13) in which the external magnetic field  $H_e$  enters directly. The variation of  $I_{\max}$  near  $H_e \approx 0$  with the external magnetic field can be estimated for narrow junctions ( $w < 2$ ).

#### 4. Numerical Methods and Their Complexity

A finite linear combination of  $X_n(y)$  and  $A_n(x)$  or  $B_n(x)$  will give an approximation of the function  $\Psi(x, y)$  by dropping all terms beyond the  $p$ th in the infinite series (20) and (37). Therefore with  $p$  here we will denote the number of modes used in the approximation.

To discretize the domain where our differential operands act we first discretize the line segments  $I_x \equiv [-\ell/2, \ell/2]$  and  $I_y \equiv [-w/2, w/2]$  by placing (assume for simplicity uniformly)  $n_x$  and  $n_y$  points respectively. Notice that a discretization of the 2D domain is defined by taking a tensor product of the above two discretizations.

We then consider the direct numerical solution of the full 2D PDE problem defined by the time independent elliptic semilinear equation (1) with the overlap boundary conditions in (2). For this purpose we used the Newton iterative method

Until  $\|\Phi^{(k+1)} - \Phi^{(k)}\| < \text{tol}$  iterate for  $k = 0, 1, \dots$

$$\nabla^2 \Phi^{(k)} - \cos(\Phi^{(k-1)})\Phi^{(k)} = \sin(\Phi^{(k-1)}) - \cos(\Phi^{(k-1)})\Phi^{(k-1)}, \quad (40)$$

which starting from an initial guess  $\Phi^{(0)}$  of the solution  $\Phi$  generates a sequence of successive approximations  $\Phi^{(k)}, k = 1, 2, \dots$ . An arbitrarily selected tolerance parameter *tol* realizes the stopping criterion. This method has been analyzed in Ref. 12 and is known to converge quadratically so that the norm of the difference between two successive iterates goes to zero in about five iterations. The main difficulty in the procedure comes from the choice of the initial guess  $\Phi^{(0)}$  which should be close enough to the solution. To obtain the  $I_{\max}(H_e)$  curve, we have started from the well known situation where  $H_e$  is very small, and the solution is close to  $\pi/2$  so that the current is close to the maximum. We have then increased the current up to the point where the iteration (40) does not converge and then proceeded to bisect between these values to find the critical current. The magnetic field is then increased, and using the solution for the previous value of  $H_e$  and  $I$ , we find the maximum current for this value of  $H_e$  by stepping and bisecting. For this to work, it is essential that the step in  $I$  and  $H$  are close and small, and we took them to be a few percent.

For the numerical solution of the Split Mode systems we need to describe the numerical techniques used to compute

- $\Phi_0$  from Eqs. (5)–(6) and (9)

- the eigenfunctions  $X_n(y)$  and
- the coefficient functions  $B_n(x)$  for  $n = 1, \dots, p$ .

Procedures for determining  $\Phi_0(y)$  can be found in Ref. 5. For the numerical calculation of the normal modes  $X_n(y)$  in (23) we need to solve the eigenvalue problem (17) numerically and for that we discretize the ODE and the boundary conditions and solve the resulting algebraic problem. Recall that we only need to compute the eigenfunctions associated with the first  $p$  even eigenpairs  $\lambda_n, X_n, n = 1, \dots, p$  (due to current symmetry odd symmetry eigenmodes do not contribute) which we appropriately normalize.

It is important to note that since one has to scan over a continuous range of currents one uses the eigenmodes for a previous value of the current in the first iteration for the next current value. We choose to vary  $H_e$  for a given current up to a critical field value, by keeping the same eigenmodes for each value of current.

To solve the system of the  $p$  1D integro-differential equations in (23)–(25) for the coefficients  $B_n$ 's we linearize the ODEs by defining a fixed point scheme obtained by splitting the differential operators into two terms, a linear and a nonlinear one as shown below

$$\begin{aligned} \frac{d^2 B_n(x)}{dx^2} + (C_{nn} - \lambda_n - r) B_n(x) = -r B_n(x) - S_n - \sum_{n'=1(n \neq n')}^p C_{nn'} B_{n'}(x) \\ + \int_{-w/2}^{w/2} X_n(y) \sin \left[ \Phi_0(y) + \sum_{n'=1}^p B_{n'}(x) X_{n'}(y) \right] dy, \end{aligned} \quad (41)$$

where in this case  $S_n \equiv \int_{-w/2}^{w/2} \sin \Phi_0(y) X_n(y) dy$ ,  $C_{nn'}$  defined in (24) and where  $r$  is a relaxation parameter to accelerate the convergence of the resulting Picard type iterative scheme defined for  $k = 0, 1, \dots$  by

$$\begin{aligned} \frac{d^2 B_n^{(k+1)}(x)}{dx^2} + (C_{nn} - \lambda_n - r) B_n^{(k+1)}(x) \\ = -r B_n^{(k)} - S_n - \sum_{n'=1}^{n-1} C_{nn'} B_{n'}^{(k+1)}(x) - \sum_{n'=n+1}^p C_{nn'} B_{n'}^{(k)}(x) + \int_{-w/2}^{w/2} X_n(y) \\ \times \sin \left[ \Phi_0(y) + \sum_{n'=1}^{n-1} B_{n'}^{(k+1)}(x) X_{n'}(y) + \sum_{n'=n}^p B_{n'}^{(k)}(x) X_{n'}(y) \right] dy. \end{aligned} \quad (42)$$

We have also used a Newton-like linearization procedure for which  $r = r_n$  with

$$r_n = \int X_n^2 \cos \left\{ \Phi_0 + \sum_{n'=1}^{n-1} B_{n'}^{(k+1)} X_{n'}^{(k+1)} + \sum_{n'=n+1}^p B_{n'}^{(k)} X_{n'}^{(k)} \right\}. \quad (43)$$

Algorithmically the proposed scheme is the following nested iteration form:

Until  $\max \|B_n^{(k+1)} - B_n^{(k)}\| < \text{tol}$  for all  $n \leq p$  iterate for  $k = 0, 1, \dots$

1. Solve the ODE system  $(d^2 B_n^{(k+1)}(x))/dx^2 + (C_{nn} - \lambda_n - r)B_n^{(k+1)}(x) = R_n^{(k+1)}$
2. Update  $R_{n+1}^{(k+1)}$  using  $B_n^{(k+1)}$ ,

where  $R_n^{(k+1)}$  is the right hand side of (42).

From the discussions in this paper so far one can conclude that we have two basic techniques to simulate an overlap 2D window Josephson junction. The first one is to solve the 2D PDE mathematical problem and the second one is to solve the system of  $p$  1D integro-differential equations. It is apparent that as one increases the number of modes  $p$  in the 1D system one obtains more accurate solutions but obviously the amount of work required to solve it numerically increases. Therefore our proposed hybrid mode expansion provides us, through its parameters  $p$ , a mechanism to arbitrarily control the accuracy of the 1D mathematical model. This mechanism is very useful since the computational complexity of the numerical process to solve the 2D PDE model is very large. In particular when one needs to qualitatively check the influence of the magnetic field — and therefore has to solve the PDE problem many times — the total amount of work can easily exhaust many of the modern computer systems. For example to obtain only the 0–1 fluxon branch in the current versus magnetic field graph using the 2D model with  $n_x = 80$  and  $n_y = 60$  (which are typical values for the discretization parameters) it took about 12 CPU hours on an IBM RS 6000.

To check the gain in efficiency using the 1D system we next perform a complexity analysis for both approaches. We start by stating that as we have observed in a series of extensive numerical experiments (using  $\text{tol} = 10^{-3}$ ) the Newton method usually requires around five iterations to converge while the Picard scheme always required less than  $5p^2$  iterations (generous upper bound). Within each iteration the 2D case involves the computation of the r.h.s of (40) and the back-substitution of a factored banded matrix obtained by discretizing the l.h.s. of (40). Within each 1D iteration one has to update the  $p$  r.h.s of (42) and then back-solve the  $p$  tridiagonal linear systems associated with the discretization of the l.h.s.. It is important to notice here that the vast amount of the computation in the 2D system is in factoring and solving the linear system while in the 1D case is in computing the integrals on the l.h.s.. Thus for the efficiency of the 1D case one needs to be very careful and update efficiently the summations involved. Assuming that  $n_x = n_y = n$  and following a tedious but elementary arithmetic count we can see that the total number of operations for the scheme (40) and the scheme (42) are approximately  $O_2 = 50n^3$  and  $O_1 = 400p^3n$ . From this we easily conclude that the 1D model is more efficient if  $p < n^{2/3}/2$ . In the case where only up to four modes are required and assuming that  $n = 60$  the 1D case is at least six times faster. The mode expansion procedure can be made very efficient by keeping the bias current constant while scanning the magnetic field. Then there is little additional computer time involved in the evaluation of the  $B_n$ 's compared to the Fourier modal amplitudes  $A_n$ . We should also note that the 1D case requires significantly less computer memory.

## 5. Numerical Results

The solution of the 2D PDE problem was obtained through an efficient implementation using the ELLPACK software,<sup>13</sup> where to obtain the maximum tunneling current we step in both current and magnetic field as described in the previous section. These results are compared with the ones obtained in our mode expansion. The one-dimensional static sine-Gordon Eq. (5) and the equations for the modal amplitudes ( $B_n$ ) were solved using MATLAB following the same approach, where for each current value (corresponding to a given  $m$  value) the magnetic field is increased till no convergence is obtained. The number of mesh points in  $x$  and  $y$  were chosen to be the same as for the 2D PDE model and the stepping in magnetic field and current were adjusted to be close.

In Fig. 2 we present the four lowest eigenvalue  $X_n$  modes for three different values of the external magnetic field ( $H_e = 0.01, 1.0, 2.0$ ) at the corresponding maximum current. We see that only for the first two modes there is a strong variation with  $H_e$ . It should be clarified of course that the dependence on the magnetic field is only indirect, in the sense that it influences the maximum possible current. The external current determines the auxiliary function  $\Phi_0(y)$  which creates the effective potential in the eigenvalue problem of (17) whose spatial variation is felt only by the low eigenvalue modes and does not influence the “high order” modes. The eigenmodes for  $H_e = 2(I_{\max} = 0)$  are identical to the cosine modes for the special case discussed in Sec. 4. For high currents there is a strong deviation from a cosine behavior for the two lowest modes. As one decreases the width  $w$  the  $X_n$  modes become cosine-like, since the maximum current density (proportional to

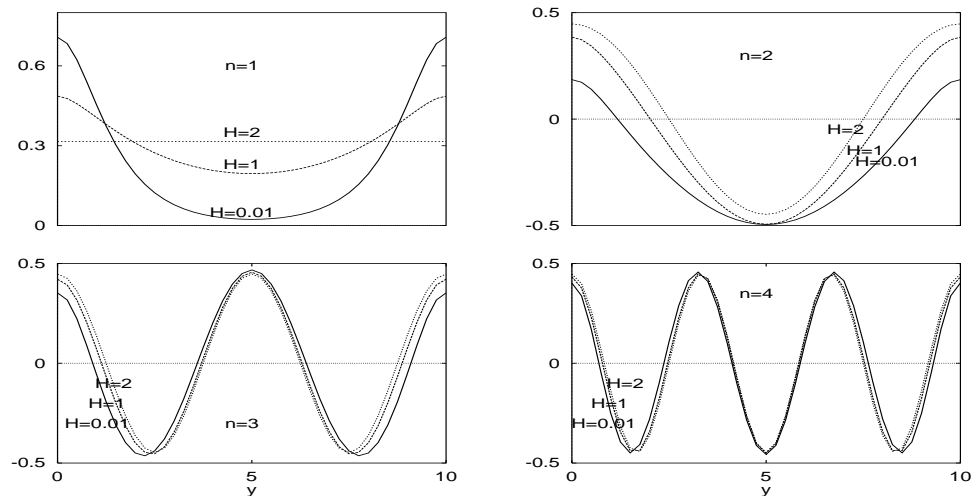


Fig. 2. Comparison of the normal  $X_n$  ( $n = 1 - 4$ ) modes for  $w = 10$  and three  $H_e$  values at 0.01 (continuous line), 1.0 (dashed), 2.0 (dotted) at the maximum tunneling current for each  $H_e$ . The  $X_n$  modes for  $H_e = 2$  are identical to the cosine modes of Sec. 4.

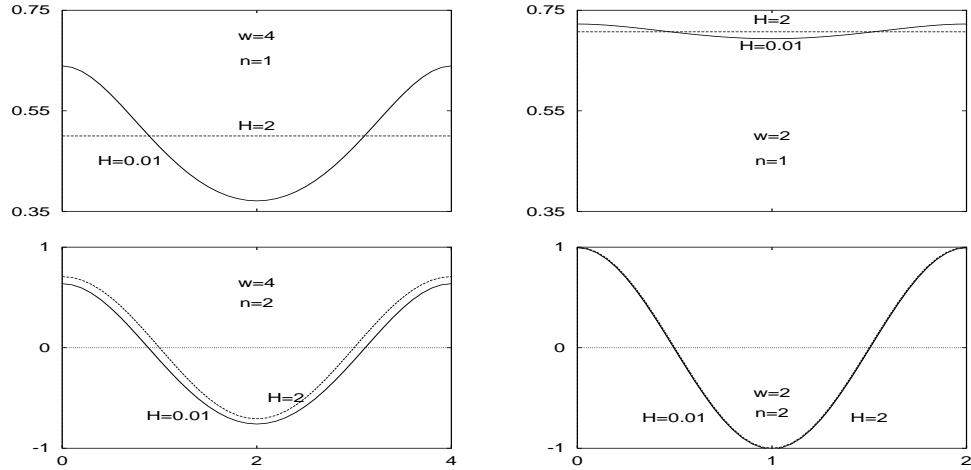


Fig. 3. Variation of the two lowest eigenvalue normal modes  $X_1$  (top) and  $X_2$  (bottom) for  $w = 4$  (left) and  $w = 2$  (right) at  $H_e = 0.01$  (continuous), 2.0 (dashed). Note that for  $w = 2$  the 2nd mode is independent of the magnetic field.

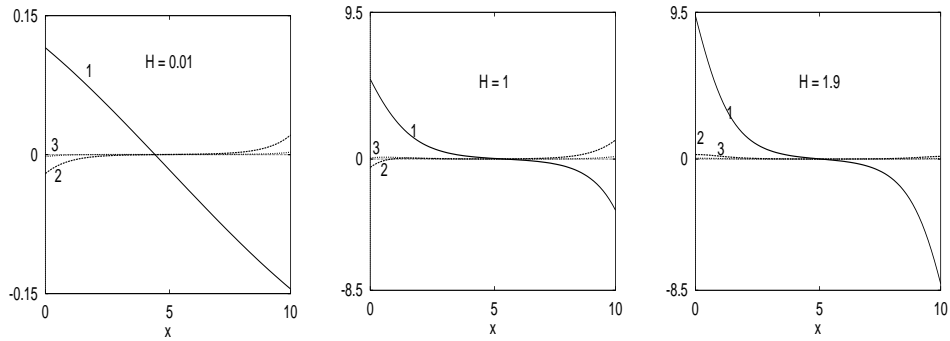


Fig. 4. The modal amplitudes  $B_n(x)$  at the maximum current solution for  $H_e = 0.01$  (left), 1.0 (middle), 1.9 (right) for  $w = 10$ . The number next to the lines is the index of the modal amplitude.

$w$  for small  $w$ ) is decreased and the variation of  $\Phi_0(y)$  along  $y$  is not significant. So in Fig. 3 we show only the lowest two eigenmodes for  $w = 4$  and  $w = 2$ , where we see a much smaller deviation from the cosine modes with  $H_e$ . In particular for  $w = 2$  the 2nd mode is exactly cosine as seen from the thick line where the results for  $H_e = 0.01$  and  $H_e = 2$  are coincident. Even for the first mode the difference is a few percent.

In Fig. 4 we plot the modal amplitudes  $B_n(x)$  ( $n = 1 - 3$ ) corresponding to the modes of Fig. 2, with  $H_e = 0.01$  (left),  $H_e = 1.0$  (center) and  $H_e = 1.9$  (right). The modes  $X_n(y)$  for  $H_e = 1.9$  are slightly different than those shown in Fig. 2 for

$H_e = 2.0$ . We see that when the current is near zero and the problem is almost 1D only the lowest  $y$ -independent mode has a significant amplitude. In all three cases the  $n = 1$  amplitude is dominant. With increasing  $I_{\max}$  or decreasing  $H_e$  the second mode also makes a contribution while at  $H_e = 0.01$ , both are relatively small since the main contribution is given by  $\Phi_0$ . We also performed the calculation with  $n = 4$  but the corresponding amplitude is not shown in the figure since it cannot be distinguished from the horizontal axis for the scale considered. It should be remarked, however that for smaller  $w$  only the  $B_1(x)$  amplitude is important as is seen in Fig. 5 for  $w = 4$  and  $w = 2$ , where the second mode is smaller by at least two orders of magnitude. In particular for  $w = 2$  it is of the order of  $10^{-6}$ . Thus, it is clear from Figs. 2–5 that as we increase  $H_e$  we go from a 1D  $y$ -dependent solution ( $\Phi_0(y)$ ) to an  $x$ -dependent solution (proportional to  $B_1(x)$ ), while for intermediate values we need more than one mode except for a small value of  $w$ , where one mode might be sufficient. In most cases even a single mode can give an estimate for the solution.

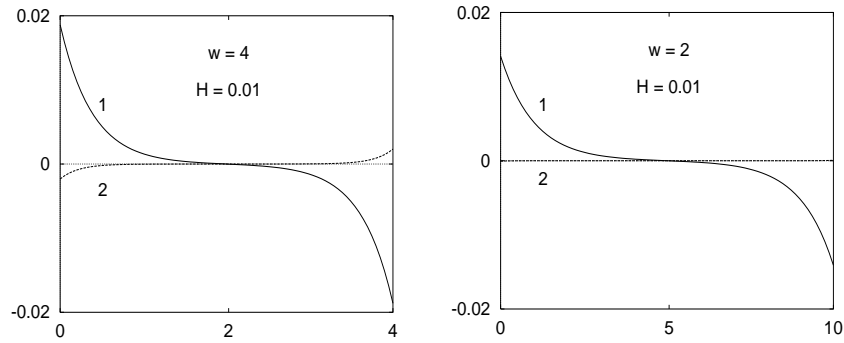


Fig. 5. The modal amplitudes  $B_1(x)$  and  $B_2(x)$  at the maximum current solution for  $H_e = 0.01$  with  $w = 4$  (left) and  $w = 2$  (right).

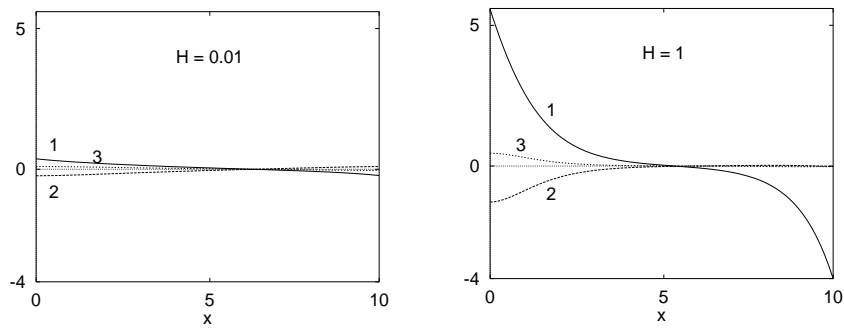


Fig. 6. The cosine amplitudes  $A_n(x)$   $n = 1 - 3$  at the maximum current solution for  $H_e = 0.01$  (left) and  $H_e = 1.0$  (right) with  $w = 10$ .

In Fig. 6 we also present the corresponding modal cosine amplitudes  $A_n$  only for the cases  $H_e = 0.01, 1.0$ . We see that a larger number of modes contributes, whose number reduces again to one at  $H_e = 2$ . At small  $H_e$  there is also some contribution from the  $n = 4$  mode (still almost an order smaller than  $B_3$ ), which is not shown in the figure.

In Fig. 7 we compare the contour plots for the phase difference  $\Phi(x, y)$  obtained from the expansion with only three modes (left part) at the external magnetic field value  $H_e = 1.0$  for which one expects the strongest deviation from 1D behavior. We chose the value of the current  $I = 25$  a little lower than the maximum current to make sure that the solutions are not close to the instability point at the maximum current and also to avoid the complication of slightly different maximum currents in different methods. The dashed lines are the numerical results obtained from the solution of the 2D problem using ELLPACK. The comparison between the two methods is quite good over the whole junction area, and some small deviations in the constant phase contours is seen in areas where the variation of  $\Phi(x, y)$  is weak which introduces sensitivity in the drawing of the contours. This is especially so because of the small number of contour levels shown (in all cases we put only 12 level lines), so that the plot is readable. In the same figure we also show in (b) the corresponding comparison using the cosine modes. We observe that the discrepancy is significant. In fact in areas where we have strong gradients and most of the energy contribution comes the agreement is very weak. In both cases the inclusion of higher modes improves things. The direct 2D calculation must be done in double precision which is very costly for the inversion of the large matrices ( $121 \times 121$ ) in the iteration procedure. In Fig. 8 we present the corresponding 3D plots of the tunneling current spatial distribution. At the values of the magnetic field  $H_e = 0.01$  and  $1.9$  the patterns are almost 1D corresponding to zero and one fluxon solutions. They are the same as in the inline geometry, while the middle case  $H_e = 1.0$  shows clearly a 2D pattern. The tunneling current is concentrated near the perimeter, along which

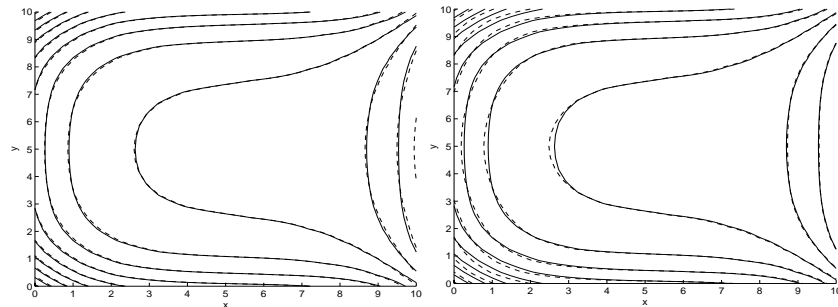


Fig. 7. Contour plots for the phase  $\Phi(x, y)$  obtained from the direct solution (dashed lines) and the mode expansion using only three  $X_n$  modes (left) for a junction with  $\ell = 10$ ,  $w = 10$ ,  $H = 1.0$  and  $I = 25$ . Also the contour lines obtained from three cosine modes (right). The solid lines are the mode expansion results in both cases.

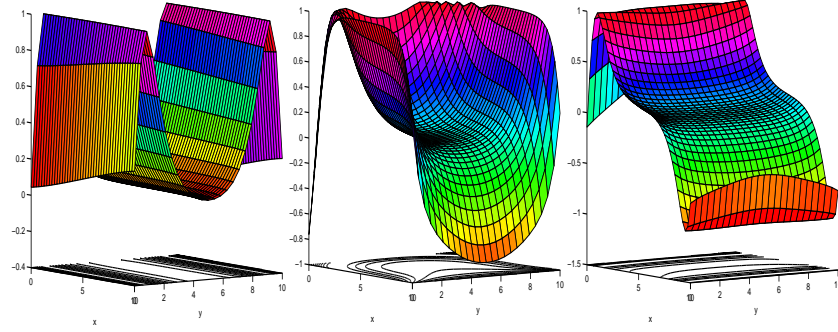


Fig. 8. 3D plot of the tunneling current distribution  $\sin \Phi(x, y)$  for  $H_e = 0.01$  (left), 1.0 (middle), 2.0 (right) and  $w = 10$ . Below we give a 2D contour projection.

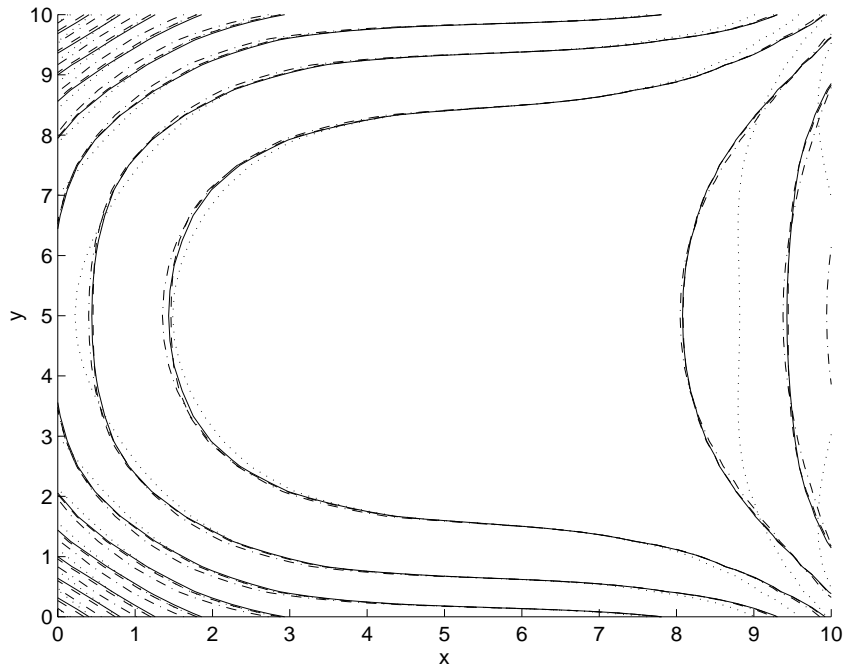


Fig. 9. Comparison of the contour plots for  $\Phi(y)$  in a wide junction  $w = 10$  with  $H = 1$  by increasing the number of modes included in the calculations with  $n = 1 - 4$  modes.

it is strongly inhomogeneous. Thus near the two left corners the phase changes by  $\pi$  within a distance equal to unity.

To check the convergence of the summation in the mode expansion we plot in Fig. 9 the constant phase contours for  $\Phi(x, y)$  by including up to  $N$  modes with  $N = 1, 2, 3, 4$  modes. We see that the inclusion of only one mode is not a good approximation for a wide junction, but the usefulness of our hybrid expansion method is that we obtain a very good approximation with only  $N = 2$  modes

while the contours for  $N = 3$  and 4 are indistinguishable. At the regions of strong gradients it is desirable to include 3 modes to get an accurate reproduction of the phase over the whole area.

To analyze the convergence of the modal expansion of the residual ( $\Psi(x, y)$ ) in (13), we have plotted the norm of each  $A_n(x)$ . This seems to scale as  $1/n^6$  for the normal modes  $X_n$  and as  $1/n^4$  for the cosines for  $n \leq 10$  which corresponds to components with significant contribution to the solution, spanning at least four orders of magnitude on a log-log scale. For the cosines there is also a prefactor which is important for small  $n$ . Of course we realize that any rigorous estimate can be done only for the large  $n$  behavior, and that since these are based on the properties of continuity and derivability of the function, we expect the same result for both, which should be like  $1/n^2$ .

In Fig. 10 we plot the maximum tunneling current as a function of  $H_e$  for three values of junction width  $w = 1, 4, 10$ . The curve with crosses (+) is the result of the direct solution of the 2D sine-Gordon equation using ELLPACK and the lines (different types for each  $N$ , i.e., the number of modes) are the results of our SFM model with only two, three and four modes. Only for  $w = 1$  is a single mode sufficient. For  $w = 4$  two modes are sufficient since the result with three

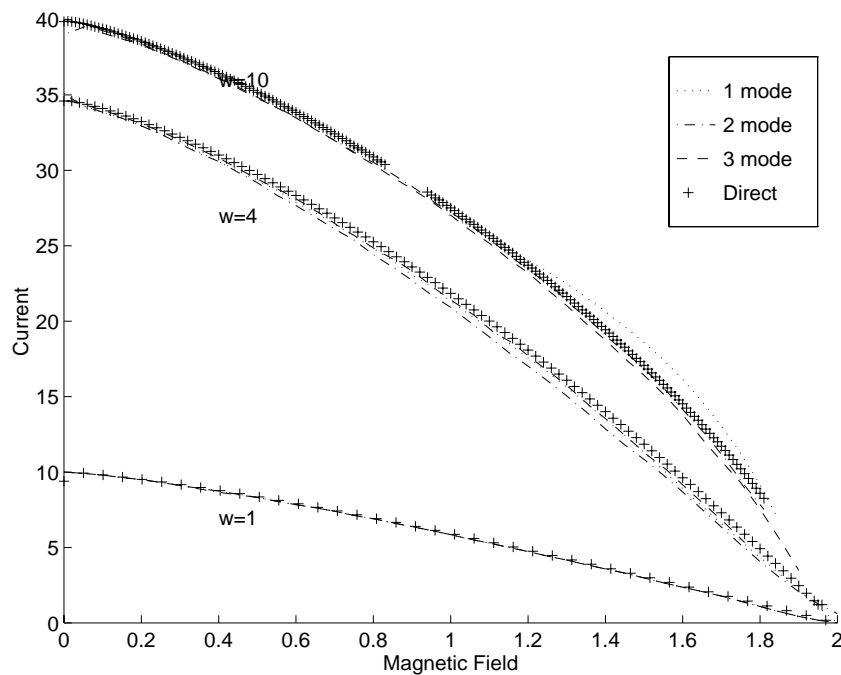


Fig. 10. Plot of the maximum tunneling current  $I_{\max}$  versus the external magnetic field  $H_e$  for  $w = 1, 4, 10$ . The lines with crosses (+) are the direct solution of the static 2D sine-Gordon Equation. For each  $w$  we give the results by including up to  $N = 1$  (dotted line), 2 (dot-dashed), 3 (dashed) modes. For  $w = 10$  the result with four modes (continuous line) is also included.

modes is indistinguishable. For  $w = 10$  we need three modes and in the figure the result for four modes coincides with that for three. We see that even for  $w = 10$  the convergence is very good and in agreement with the direct 2D discretization solution. Near  $H = 0$  we see a saturation of the maximum current as expected while all curves coalesce at  $H = 2$ , where the maximum current vanishes and the boundary conditions are inline (1D). The slope of the curve near  $H = 2$  is  $dI_{\max}/dH = (2/\pi)\ell w$ , which is in agreement with the calculations for  $w < 4$ . While for small  $w$  near  $H_e = 2$  the effect will be proportional to the junction width again there is a saturation for large  $w$ . It should be emphasized that the case  $w = 10$  is impossible to treat in the usual effective 1D model,<sup>6,7</sup> except near  $H_e = 2$ . The situation is not as promising if we use the cosine set of modes for  $w = 10$  as in Fig. 11. In fact the inclusion of only one mode gives a totally wrong result at small magnetic fields. The fact that the curve does not start from  $H_e = 0$  is because the maximum current density over which we scan is the one obtained from the solution of the auxiliary equation for  $\Phi_0(y)$  and for large  $w$  is given by (12) and always less than 4. This expression takes into account the saturation with  $w$  due to the exclusion of magnetic flux from the center. When we use a single mode though the total current is evenly spread over the whole width  $w = 10$  so that the current density in the single mode equation (37) given by  $S_0$  is much lower than the critical

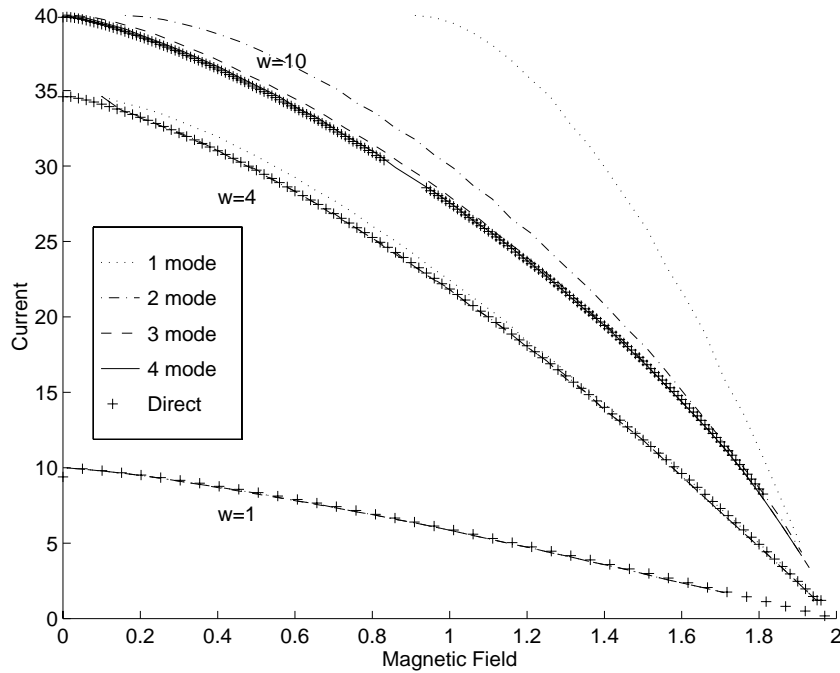


Fig. 11. Same as Fig. 10 but using the cosine modes.

value. In the usual 1D model<sup>6,7</sup> at zero magnetic field the total tunneling current for narrow junctions is equal to the total surface, so that the result would be that for  $w = 1$  multiplied by 10. In our modified 1D model we include the effect of the second dimension in (37), so that it deviates also from the usual 1D result. Also even with four modes the convergence is not as fast as for the  $X_n$  modes.

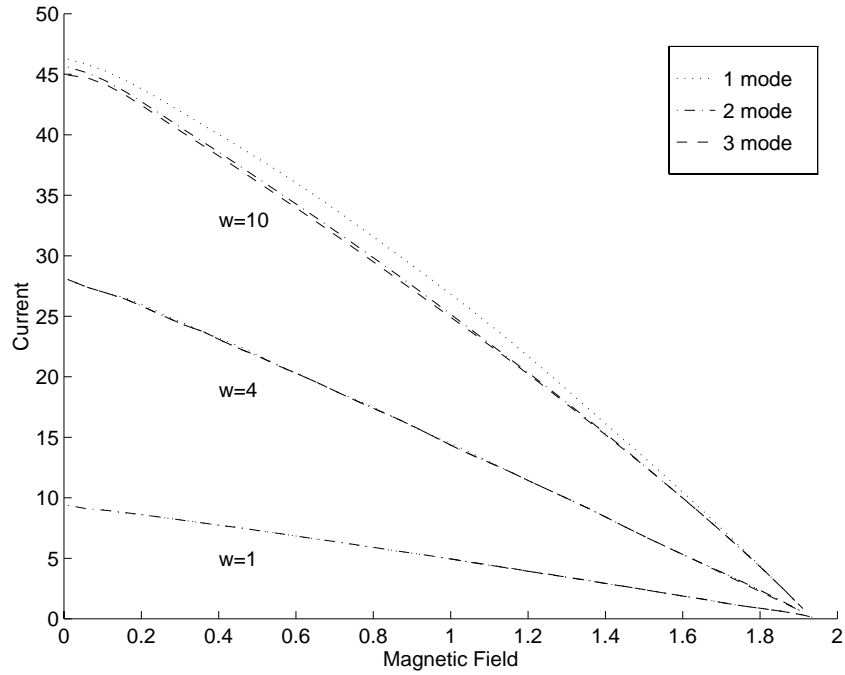


Fig. 12. Same as Fig. 11 but for symmetric boundary conditions.

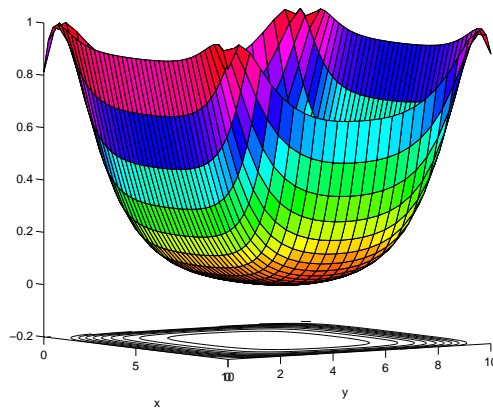


Fig. 13. 3D plot of the tunneling current distribution  $\sin \Phi(x, y)$  for  $H_e = 0.1$  and  $w = 10$ , with symmetric boundary conditions. Below we give a 2D contour projection.

In Fig. 12 we calculate the maximum tunneling current in the case of symmetric boundary conditions, i.e.,  $(\partial\Phi/\partial x)|_{x=\pm\ell/2} = H_e \pm I_d/2$  and  $(\partial\Phi/\partial y)|_{y=\pm w/2} = \pm I_d/2$ , where  $I_d = I/(\ell + w)$ . This gives the possibility to consider the situation where the current is peaked at the corners. Now there is much less curvature in Fig. 11 near  $H = 0$  due to the in-like component of the bias current. The values of  $I_d$  at  $H = 0$  for  $w = 1, 4, 10$  are  $I_d = 0.74, 2.0, 2.25$  correspondingly. It is lower than for the overlap case, where  $I_d = I/\ell = 4.0$  for  $w = 4$ . This is due to the effect at the corners, where the current that flows from both directions will tunnel through the same area from the corner, which has a radius of the order of 2 (in units of  $\lambda_J$ ) as is seen in Fig. 13. On the other points maximum tunnel current density (per unit area) is unity. Of course for both types of BC the curves coalesce at the same point in  $H$  for  $I_{\max}$  near zero.

## 6. Conclusions

In this paper we presented the split mode method and applied it to solving the 2D elliptic sine-Gordon equation describing a Josephson junction with overlap current feed. The method relies on an auxiliary 1D problem which can be solved analytically. We showed by direct comparison with the numerical solution of the 2D problem that the SMM is easy to implement, converges and can be made arbitrarily precise. Since this method involves solving a generally small number of ordinary differential equations it is much less computationally intensive than the 2D numerical calculation. This is especially true for the large values of the width  $w$  for which the 2D problem needs to be solved in double precision.

We have also compared the convergence of the expansion of the residual  $\Psi$  using cosine modes and the normal modes associated to the auxiliary problem, and found a faster convergence for the latter. For  $w = 10$  we find a good agreement with two normal modes while three cosine modes are necessary to obtain the same result. Finally we believe that this method could be applied with fruitful results to other types of semilinear problems with symmetric boundary conditions like the Klein-Gordon or the nonlinear biharmonic equations.

## References

1. N. N. Yanenko, *The Method of Fractional Steps* (Springer-Verlag, New York, 1971).
2. A. Quarteroni and A. Valli, *Numerical Approximation of Partial Differential Equations* (Springer-Verlag, New York, 1994).
3. G. Adomian, *Solving Frontier Problems of Physics: The Decomposition Method* (Kluwer, Dordrecht, 1994).
4. E. Y. Deeba and S. A. Khuri, *J. Comp. Physics* **124**, 442–448 (1996).
5. J. G. Caputo, N. Flytzanis, Y. Gaididei, and E. Vavalis, *Phys. Rev.* **E54**, 2092 (1996).
6. A. Barone and G. Paterno, *Physics and Applications of the Josephson Effect* (John Wiley, 1982).
7. S. Pagano, B. Ruggiero, and E. Sarnelli, *Phys. Rev.* **B43**, 5364 (1991).
8. G. A. Maugin, H. Hadouaj, and B. Malomed, *Phys. Rev.* **B45**, 9688–9694 (1991).
9. L. Lui and J. Prost (eds.), *Solitons in Liquid Crystals* (Springer Verlag, 1991).

10. C. S. Owen and D. Scalapino, *Phys. Rev.* **164**, 538 (1967).
11. M. Abramowitz and I. A. Stegun, *Handbook of Mathematical Functions* (Dover Publications, Inc., New York, 1972).
12. J. G. Caputo, N. Flytzanis, and E. Vavalis, *Int. J. Mod. Phys.* **C6**, 241 (1995).
13. J. Rice and R. Boisvert, *Solving Elliptic Problem Using ELLPACK* (Springer-Verlag, 1985).